Comparison of the Dynamical Structures of Lipoamide Dehydrogenase and Glutathione Reductase by Time-Resolved Polarized Flavin Fluorescence[†]

Philippe I. H. Bastiaens,[‡] Arie van Hoek,[§] Willem F. Wolkers,[‡] Jean-Claude Brochon,[∥] and Antonie J. W. G. Visser[*,‡]
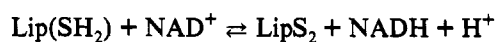
Departments of Biochemistry and Molecular Physics, Agricultural University, P.O. Box 8128, 6700 ET Wageningen, The Netherlands, and Laboratoire pour l'Utilisation du Rayonnement Electromagnétique, CNRS–CEA–MENJS, Centre Universitaire Paris-Sud, Orsay F91405, France

ABSTRACT: Time-resolved polarized fluorescence spectroscopy has been applied to the bound FAD in the structurally related flavoproteins lipoamide dehydrogenase from *Azotobacter vinelandii* (LipDH-AV) and glutathione reductase (GR) from human erythrocytes. The fluorescence parameters as obtained from the maximum entropy analysis differ considerably in both enzymes, reflecting the unique properties of the flavin microenvironment. Three conformational substates are revealed in LipDH-AV and five in GR. Almost 90% of the population of GR molecules has a fluorescence lifetime in the order of 30 ps which originates from efficient exciplex formation with Tyr197. Equilibrium fluctuations between conformational substates are observed for LipDH-AV on a nanosecond time scale in the temperature range 277–313 K. Interconversion between conformational substates in GR is slow, indicating that large activation barriers exist between the states. In agreement with these results, a model is postulated which ascribes a role in catalysis to equilibrium fluctuations between conformational substates in GR and LipDH-AV. From time-resolved fluorescence anisotropy as a function of temperature, distinction can be made between flavin reorientational motion and interflavin energy transfer. In both proteins intersubunit energy transfer between the prosthetic groups is observed. Furthermore, it is revealed that only the flavin in glutathione reductase exhibits rapid restricted reorientational motion. Geometric information concerning the relative orientation and distance of the flavins can be extracted from the parameters describing the energy-transfer process. The obtained spatial arrangement of the flavins is in excellent agreement with crystallographic data.

Lipoamide dehydrogenase (LipDH)[1] and glutathione reductase (GR) are both members of the family of disulfide oxidoreductases. These flavoproteins have FAD as a prosthetic group and a redox-active disulfide in common (Williams, 1976). The proteins with a molecular mass of 100 kDa have a dimeric quaternary structure (Worthington & Rosemeyer, 1974; Schulz et al., 1975). The catalytic site comprises amino acid residues from both subunits, which explains why the physiological enzymatic activity is abolished upon monomerization of the enzymes (Kalse & Veeger, 1968; Karplus & Schulz, 1987; Schierbeek et al., 1989; Mattevi et al., 1991; van Berkel et al., 1991). LipDH is part of the multienzyme pyruvate dehydrogenase and 2-oxoglutarate dehydrogenase

complexes catalyzing the oxidation of covalently bound dihydrolipoamide coupled to the reduction of NAD+ (Reed, 1974):

$$Lip(SH_2) + NAD^+ \rightleftharpoons LipS_2 + NADH + H^+$$

GR operates as a dimer in erythrocytes where it maintains a high value for the ratio of reduced to oxidized glutathione concentrations which is, among others, essential for proper function of erythrocytes by stabilizing thiols in the cell membrane. The enzyme utilizes NADPH instead of NADH and, in contrast to LipDH, irreversibly oxidizes the cofactor under physiological conditions (Williams, 1976):

$$GSSG + NADPH + H^+ \rightarrow 2GSH + NADP^+$$

The genes of lipoamide dehydrogenase from *Azotobacter vinelandii* (LipDH-AV) and glutathione reductase from *Escherichia coli* have been cloned and brought to expression (Westphal & de Kok, 1988; Schulze et al., 1991; Berry et al., 1989). Relatively large quantities of the enzymes can be made available, and the active site can be modified by site-directed mutagenesis. The crystal structure of GR from human erythrocytes has been refined to 1.54 Å and, recently, the structure of LipDH-AV to 2.2 Å, enabling detailed comparison of both structures (Karplus & Schulz 1987; Mattevi et al., 1991). Small differences in tertiary and quaternary structure were revealed. The relative orientations of the NAD(P)+- and FAD-binding domains differ by a tilt angle of 7–8°.

[*] Author to whom correspondence should be addressed.
[‡] Department of Biochemistry, Agricultural University.
[§] Department of Molecular Physics, Agricultural University.
[∥] CNRS–CEA–MENJS.
[1] Abbreviations: EB, erythrosine B; EDTA, ethylenediaminetetraacetic acid; FAD, flavin adenine dinucleotide; GR, glutathione reductase; GSSG, oxidized glutathione; GSH, reduced glutathione; LipS$_2$, oxidized lipoamide; Lip(SH$_2$), reduced lipoamide; LipDH, lipoamide dehydrogenase; LipDH-AV, lipoamide dehydrogenase from *Azotobacter vinelandii*; MEM, maximum entropy method; NAD(P)+, nicotinamide adenine dinucleotide (phosphate), oxidized form; NAD(P)H, nicotinamide adenine dinucleotide (phosphate), reduced form; SDS–PAGE, sodium dodecyl sulfate–polyacrylamide gel electrophoresis; TCSPC, time-correlated single-photon counting; Tyr, tyrosine.

Furthermore, the relative position of the subunits differs by a translational shift of 4.4 Å, which results in a much narrower binding cleft for lipoamide as compared to the glutathione-binding site. It was postulated that this narrow binding cleft facilitates binding of the long aliphatic arm of the covalently bound substrate which is able to move between the catalytic centers of the different enzymes of the multienzyme complex (Mattevi et al., 1991).

LipDH-AV contains a C-terminal extension of 15 amino acids which is not present in GR. The last 10 amino acid residues are not visible in the electron density map, indicating that this polypeptide is highly flexible or disordered (Mattevi et al., 1991). Removal of the last 14 amino acids by site-directed mutagenesis results in inactivation of the enzyme. In addition, the deletion mutant (LipDH-Δ14) has a tendency to dissociate into monomers (K_d = 2.5–5.0 μM instead of 1 nM for wild type enzyme), which demonstrates that the C-terminal polypeptide is essential for interaction between the subunits (Schulze et al., 1991).

The fluorescence properties of FAD bound to GR and LipDH differ considerably (de Kok & Visser, 1987). The fluorescence quantum yield of FAD bound to GR is 7.7% of that of FAD bound to LipDH. Time-resolved fluorescence studies of the flavin in GR at 20° revealed a highly inhomogeneous fluorescence decay. At least 4 different lifetimes were needed to describe the fluorescence decay ranging from 50 ps to 5.5 ns. The fluorescence decay of LipDH could be fitted to a sum of three exponentials. Most remarkable was the difference in time-resolved fluorescence anisotropy in both proteins. Almost complete depolarization of the fluorescence was attained in GR with a correlation time of 3.6 ns. A predominantly long correlation time, reflecting protein tumbling, was found for LipDH. In addition, a small-amplitude process with a correlation time in the order of 10 ns could be resolved. These results were interpreted to arise from different dynamic behavior of the flavin in GR and LipDH. The shorter correlation time with a large amplitude supports a highly mobile prosthetic group in GR whereas the flavin is apparently more rigidly bound in LipDH.

In this paper we report on a detailed time-resolved fluorescence and fluorescence anisotropy study of FAD in GR and LipDH-AV. Our purpose was to obtain insight into the structural and dynamic properties of these proteins as monitored by the polarized fluorescence decay at different temperatures. The basis of this approach was that inhomogeneity in the environment of the chromophore will lead to a range of excited-state processes and therefore will give rise to nonexponential fluorescence decay (Beechem & Brand, 1985). Due to this property it is in principle possible to monitor conformational substates in proteins and their dynamic exchange (Austin et al., 1975; Frauenfelder & Gratton, 1986; Frauenfelder et al., 1988). In multiflavin-containing proteins it can be expected that homoenergy transfer takes place. It is then of importance to be able to separate this contribution to the depolarization of the fluorescence from that arising from reorientational dynamics (Bastiaens et al., 1988, 1989, 1991; Kalman et al., 1991).

The classical description of the fluorescence decay by a discrete set of lifetimes has both mathematical and physical disadvantages (Livesey & Brochon, 1987). The inverse Laplace transform of the fluorescence decay is recovered in the maximum entropy method (MEM) by fitting the decay to a function composed of a large number (up to 200) of exponentials (Livesey & Brochon, 1987; Mérola et al., 1989; Gentin et al., 1990). The advantage of this method is that one obtains a unique solution and that no a priori knowledge of the distribution model is needed. This type of analysis is well suited for complex decays encountered in biological molecules where multiple conformations of different tiers give rise to semicontinuous sets of lifetime distributions (Frauenfelder & Gratton, 1986; Alcala et al., 1987).

MATERIALS

LipDH-AV was expressed in *E. coli* TG2 and purified according to published procedures (Westphal & de Kok, 1988). The enzyme preparations were frozen in liquid nitrogen and stored at –70 °C in 100 mM potassium phosphate buffer, 0.5 mM EDTA, pH 7.0. GR was isolated from erythrocytes obtained from 7.5 L of human blood according to published procedures (Krohne-Ehrich et al., 1971). The final preparation had a specific activity of 147 units/mg at 20 °C and a 280/460-nm ratio of 6.0. The enzyme was pure as judged by SDS–PAGE. The preparation was stored in 50 mM potassium phosphate buffer, 200 mM KCl, 1 mM EDTA, 14 mM 2-mercaptoethanol, pH 7.0 at 4 °C. In the morning of an experiment, the samples were brought to room temperature and chromatographed on a Biogel PGD-6 column (1 × 6 cm, Bio-Rad) equilibrated with 50 mM potassium phosphate buffer, pH 7.0, in nanopure-grade water. In that way unbound FAD is removed from the samples. The enzyme preparations were brought to 80% (v/v) glycerol by gently mixing 100 μL from the eluted sample with 400 μL of 100% glycerol (Merck, fluorescence microscopy grade) until a homogeneous solution was obtained. All final preparations had a concentration of 10–15 μM on the basis of FAD light absorption at 457 nm (Westphal & de Kok, 1988). When the samples were frozen to 243 K, a clear transparent glass was formed with no indications of any precipitate.

METHODS

Time-Resolved Fluorescence. Fluorescence decay and fluorescence anisotropy decay curves were measured by the time-correlated single-photon-counting (TCSPC) technique (O'Connor & Phillips, 1984). The TCSPC apparatus, consisting of an argon ion laser and associated optics and detection electronics, has been described elsewhere (van Hoek et al., 1987). The excitation wavelength was 457.9 nm, close to the absorption maximum of the first electronic transition of the bound flavin. Emission was passed through a combination of a KV 550 cutoff and 557.9 interference filter of 10-nm bandpass (Schott). The temperature in the sample housing was controlled by a liquid nitrogen flow setup with a temperature controller (Oxford Model ITC4). The instrumental function, corresponding to the laser pulse convoluted with the detection response, was determined by measuring the fluorescence decay of a fast reference compound (erythrosine B in water). The lifetime of this compound is slightly dependent on temperature and amounts to approximately 80 ps. The exact value of the reference lifetime at a certain temperature was determined by iterative reconvolution with a compound having a longer fluorescence lifetime (erythrosine B in methanol, lifetime ≈500 ps). Flavin fluorescence was sampled during 10 cycles of 10 s in each polarization direction where the detection frequency of the parallel polarized component was set to 30 kHz to prevent pulse pileup. The pulse mimic was sampled for two or three cycles of 10 s in each polarization direction until an approximate peak count of 20–30 kilocounts was reached in the parallel component. One complete measurement consisted of measuring the polarized fluorescence decays of the reference

compound, the sample, the background, and again the reference compound. Background fluorescence was sampled at one-fifth of the sample acquisition time; it was always below 2% of the fluorescence intensity of the LipDH samples but amounted to 2–5% in the GR samples due to the lower quantum yield of this protein.

Data Analysis. Analysis of total fluorescence decay $I(t)$ and anisotropy decay $r(t)$ was performed using the commercially available maximum entropy method (Maximum Entropy Data Consultants Ltd., Cambridge England). The principle of MEM has been described in the literature (Livesey & Brochon, 1987) and will be shortly outlined below in relation to our application. In all the experiments, the parallel $I_\parallel(t)$ and perpendicular $I_\perp(t)$ fluorescence intensity components were acquired after excitation with vertically polarized light. The image $\alpha(\tau)$ of the total fluorescence intensity $i(t)$, after δ-pulse excitation, is given by the inverse Laplace transform:

$$i(t) = i_\parallel(t) + 2gi_\perp(t) = \int_0^\infty \alpha(\tau)e^{-t/\tau}\,d\tau \qquad (1)$$

The g-factor was found to be equal to 1 in our TCSPC apparatus (van Hoek et al., 1907). The image $\alpha(\tau)$ is recovered by maximizing the Skilling–Jaynes entropy function S_{SJ} (Livesey & Brochon, 1987)

$$S_{SJ} = \int_0^\infty \alpha(\tau) - m(\tau) - \alpha(\tau)\log(\alpha(\tau)/m(\tau))\,d\tau \qquad (2)$$

and minimizing the χ^2 data fit criterium

$$\chi^2 = \frac{1}{M}\sum_{k=1}^M ((I_k^{calc} - I_k^{obs})/\sigma_k)^2 \qquad (3)$$

where $m(\tau)$ is the starting model of the distribution chosen to be flat in log τ space when there is no a priori knowledge about the system, as this introduces the least correlation between the parameters $\alpha(\tau)$. The superscripts calc and obs on I denote the observed and calculated intensities in channel k of the multichannel analyzer. M is the total amount of channels used in the analysis of the fluorescence decay (typically 1024 channels) and σ_k^2 is the variance in channel k. For an optimal fit of the data, χ^2 should approach unity.

In practice, 150 equally spaced values on a log τ scale (between 0.01 and 10 ns) were used in the analysis of $i(t)$. In order to recover the proper lifetime image of GR in aqueous solution, we had to introduce a negative shift of −0.5 channel in the analysis corresponding to a delay of about 10 ps in the excitation pulse (relative to the fluorescence profile). This shift can be rationalized by the fact that neutral density filters had to be introduced in the measurement of the pulse profile, which were absent in the measurement of the fluorescence decay of the sample. These additional filters give rise to a time delay owing to the increase of the refractive index relative to air. Because of the low fluorescence quantum yield of GR, neutral density filters were omitted in order to achieve a higher excitation intensity to reach a detection frequency of 30 kHz. In the LipDH samples, the optical path of reference and sample were identical and no shift was introduced in the analysis.

One is able to recover from fluorescence anisotropy experiments the complete three-dimensional image given by $\gamma(\tau,\phi,r_0)$, representing the number of fluorophores with lifetime τ, rotational correlation time ϕ, and initial anisotropy r_0. This image is related to the parallel $i_\parallel(t)$ and perpendicular $i_\perp(t)$ polarized components of the fluorescence

after deconvolution by (Livesey & Brochon, 1987):

$$i_\parallel(t) = \frac{1}{3}\int_0^\infty \int_0^\infty \int_{-0.2}^{0.4} \gamma(\tau,\phi,r_0)e^{-t/\tau}(1 + 2r_0e^{-t/\phi})\,d\tau\,d\phi\,dr_0 \qquad (4)$$

$$i_\perp(t) = \frac{1}{3}\int_0^\infty \int_0^\infty \int_{-0.2}^{0.4} \gamma(\tau,\phi,r_0)e^{-t/\tau}(1 - r_0e^{-t/\phi})\,d\tau\,d\phi\,dr_0 \qquad (5)$$

The Skilling–Jaynes entropy function S_{SJ} has the same form as in eq 2 except that $\alpha(\tau)$ is replaced by $\gamma(\tau,\phi,r_0)$ and integration is performed over the three dimensions τ, ϕ, and r_0. If one assumes a priori that there is no correlation between τ and ϕ (nonassociative modeling), the images $\alpha(\tau)$ and $\beta(\phi)$ can be separated in eq 4 and 5 as shown for the parallel fluorescence intensity component:

$$i_\parallel(t) = \frac{1}{3}\int_0^\infty \alpha(\tau)e^{-t/\tau}\,d\tau \int_0^\infty (1 + 2\beta(\phi))e^{-t/\phi}\,d\phi \qquad (6)$$

The integrated amplitude $\beta(\phi)$ corresponds to the initial anistropy r_0. From this type of one-dimensional anisotropy analysis one obtains a spectrum of amplitudes β against correlation times ϕ. Similar considerations regarding the starting model in the recovery of $\alpha(\tau)$ apply to the recovery of $\beta(\phi)$; i.e., if there is no a priori knowledge of the distribution, one should start with a flat spectrum in log ϕ space.

In the global fit of $i_\parallel(t)$ and $i_\perp(t)$, a fixed image of the fluorescence decay consisting of 150 equally spaced values in log τ space was introduced in the analysis. The starting model of $\beta(\phi)$ consisted of 100 uniform and equally spaced values on a log ϕ scale (from 0.1 to 100 ns).

The fluorescence parameters as calculated from the images $\alpha(\tau)$ and $\beta(\phi)$ have been obtained as follows. The average fluorescence lifetime of a sample $\langle\tau\rangle$ is defined as

$$\langle\tau\rangle = \sum_i^N \alpha_i\tau_i / \sum_i^N \alpha_i \qquad (7)$$

where the summation is carried out over the whole range (N) of τ_i values of an $\alpha(\tau)$ spectrum. The barycenter of a peak in the spectrum is determined in a similar fashion except that the summation is carried out over a limited range of τ_i values encompassing a local peak (Mérola et al., 1989). A peak is defined as a range of $\alpha(\tau)$ values containing a local maximum and delimited by two minima. The fractional area of a peak is the ratio between the integrated peak intensity and the total intensity of the spectrum. Similar parameters can be determined from the $\beta(\phi)$ image where the axes are replaced by ϕ and β instead of τ and α.

The time-resolved fluorescence anisotropy of the proteins at different temperatures was also analyzed with the commercially available global analysis software package (Globals Unlimited, Urbana, IL). The parallel and perpendicular polarized fluorescence decays at the different temperatures were simultaneously analyzed to a single-decay model encompassing temperature-invariant parameters. These parameters were linked as given in the Results section. Errors in the parameters were determined at a 67% confidence interval by a rigorous error analysis (Beechem & Gratton, 1988; Beechem et al., 1991).

RESULTS

Total Fluorescence Decay Analysis. In Figure 1, the time-resolved fluorescence profiles are shown for LipDH-AV and GR in aqueous solution at room temperature. Both decays are entirely different and have a strong heterogeneous
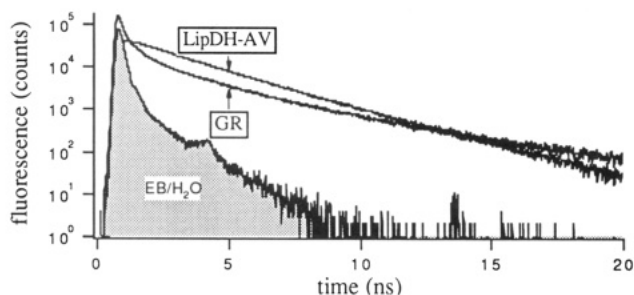
FIGURE 1: Experimental total fluorescence decay of LipDH-AV and GR in 50 mM potassium phosphate buffer at pH 7.0 and 293 K: excitation at 457.9 nm, emission at 550 nm. The fluorescence response of the pulse mimic erythrosine B in water (EB/H$_2$O) is also shown.
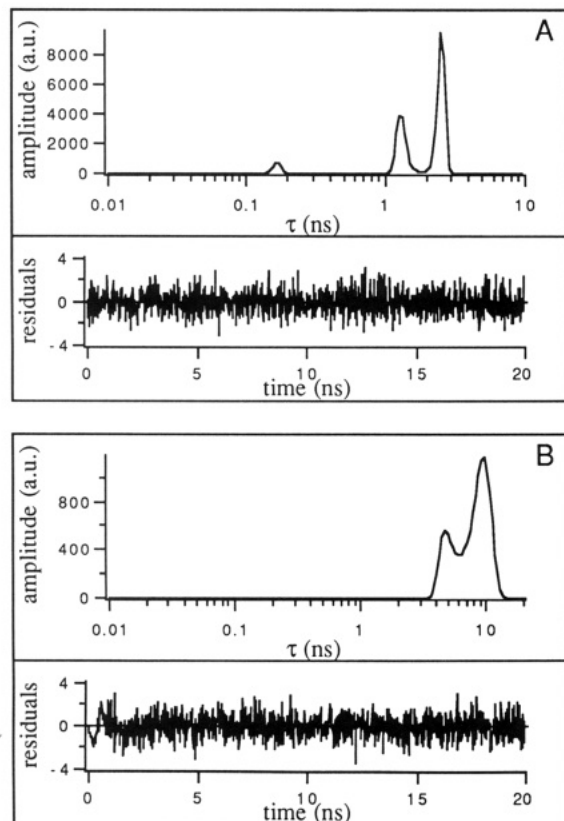

FIGURE 2: Inverse Laplace transform of fluorescence decay of LipDH-AV in 50 mM potassium phosphate buffer at pH 7.0 at 293 K (A) and in 80% glycerol, 50 mM potassium phosphate buffer at pH 7.0 at 243 K (B). The weighted residuals of the fit are placed in the boxes under the lifetime spectra.

character. The inverse Laplace transform of the fluorescence decay of FAD bound to LipDH-AV in aqueous solution consists of three peaks (Figure 2A). At 277 K the image is dominated by a peak with a barycenter at 3.2 ns. Above 283 K, the relative contributions of the shorter lifetime classes increase at the expense of the longer one (Figure 3B). The increase of the fractional contribution of the two shorter components implies that states of the protein with higher conformational energy are populated. Since the barycenters of the lifetime classes converge (Figure 3A), interconversion between conformational states takes place on a time scale comparable to the excited-state lifetime. The amplitudes and lifetimes are then eigenvectors and eigenvalues of a system of three coupled linear differential equations (Alcala et al., 1987). In that case, the fractional contributions of the lifetime classes cannot be used to calculate the fractional population of the conformational states.
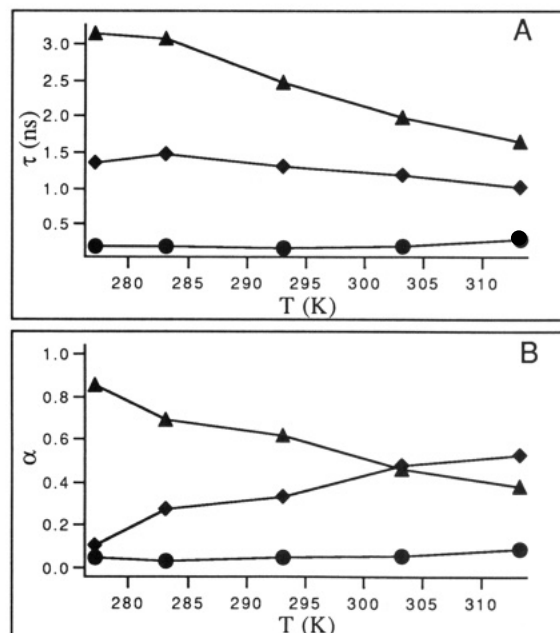

FIGURE 3: Temperature dependence of barycenters (A) and fractional contributions (B) of the lifetime classes in LipDH-AV in 50 mM potassium phosphate buffer at pH 7.0.

A bimodal instead of a trimodal distribution is recovered for the protein in 80% glycerol at 243 K (Figure 2B). The conformation associated with the short-lifetime class (0.15 ns) is not populated at this temperature in 80% glycerol, suggesting that this state of the protein has the highest conformational energy. The barycenters of the two observed states in 80% glycerol are shifted to longer lifetimes as compared to the lifetime classes in aqueous solution. Since rapid protein fluctuations are damped in cryogenic solvents at low temperature (Gavish & Werber, 1979), it is expected that the fluorescence lifetime of protein-bound flavin is longer due to diminished collisional quenching by neighboring amino acid residues. The temperature dependence of the lifetime classes is then determined by two factors: (i) the activation barrier between conformational states and (ii) the effective activation energy of collisional quenching. The activation energies of the two processes differ by at least 1 order of magnitude and can be ascribed to equilibrium fluctuations of different tiers (Frauenfelder & Gratton, 1986; Frauenfelder et al., 1988). The interplay of both mechanisms makes the system too complex to analyze using quantitative global analytical methods which are able to extract the activation energies (Ameloot et al., 1986; Boens et al., 1989).

Up to five peaks could be distinguished in the spectrum of GR, which is dominated by a short-lifetime component with a barycenter positioned at 30 ps (Figure 4A). The barycenters of the different lifetime classes were invariant to temperature (Figure 5A), implying that exchange between conformational states is slow in this temperature range in contrast to LipDH-AV. The normalized integrated amplitudes then correspond to the fractional population of the protein substates. From the fractional populations of the lifetime classes the standard enthalpy difference ΔH_i^0 between states can be estimated with van't Hoff's law:

$$-(\Delta H_i^0/R) = (d \ln (\alpha_i/\alpha_1))/d(1/T) \qquad (8)$$

where α_1 is the integrated amplitude of the shortest lifetime component (30 ps), α_i is the integrated amplitude of another component i, R is the gas constant (8.31 J K^{-1} mol^{-1}), and T is the temperature in kelvin. So the enthalpy of the confor-
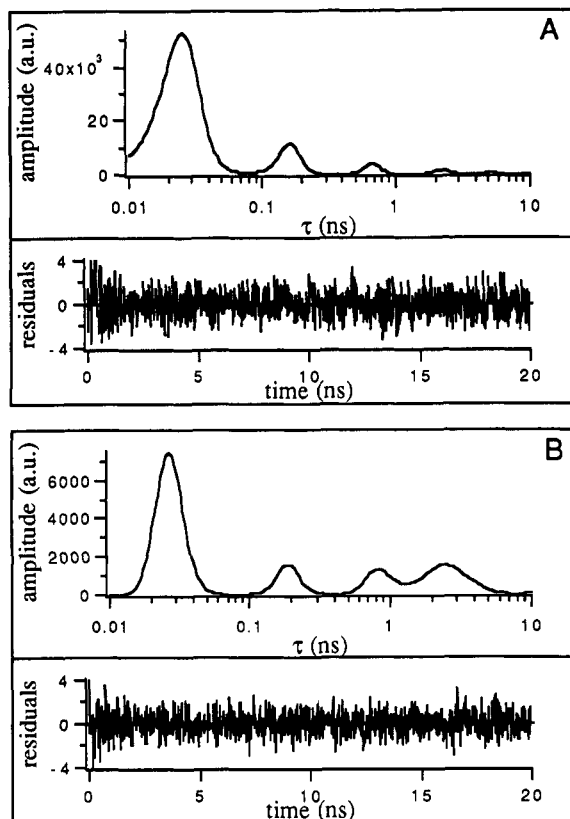
FIGURE 4: Inverse Laplace transform of fluorescence decay of GR in 50 mM potassium phosphate buffer at pH 7.0 at 293 K (A) and in 80% glycerol, 50 mM potassium phosphate buffer at pH 7.0 at 243 K (B). The weighted residuals of the fit are placed in the boxes under the lifetime spectra.
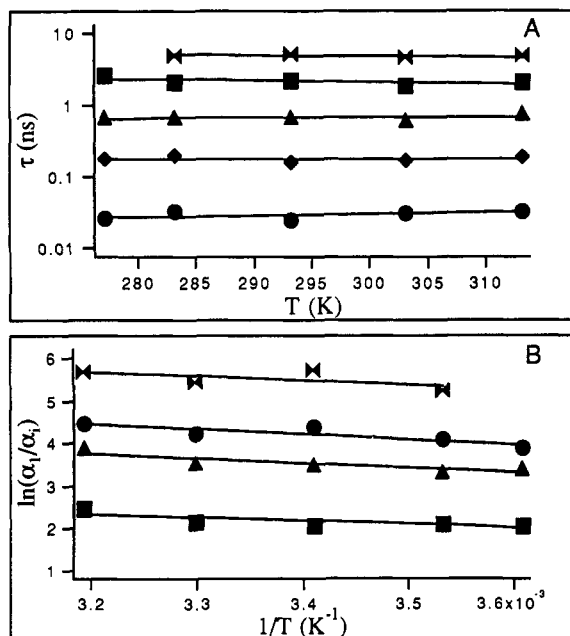

FIGURE 5: Temperature dependence of barycenters and relative populations of GR molecules in 50 mM potassium phosphate buffer at pH 7.0: (A) semilogarithmic plot of barycenters of the lifetime classes as function of temperature; (B) van't Hoff plot of conformational transition equilibrium constants ($K = \alpha_1/\alpha_i$).

mational states can then be calculated relative to the most populated state (30 ps), which we assigned a relative value of 0 kJ/mol (Figure 5B). In this way, part of the protein energy landscape can be drawn (Figure 6). The large error bars on the enthalpies are due to the small values of the fractional populations with longer lifetimes. The activation barriers
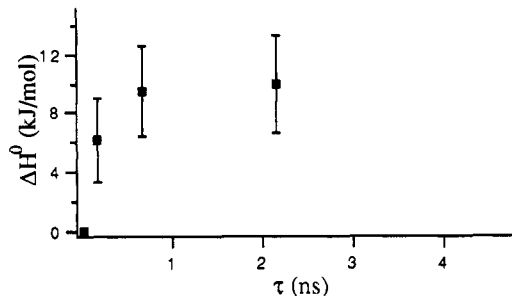

FIGURE 6: Standard free enthalpy of conformational transition in GR. The conformational coordinate is replaced by the barycenter of the lifetime classes on the x-axis. The enthalpy is relative to the conformational state associated with the smallest lifetime class (30 ps), which was assigned a value of 0 kJ/mol.
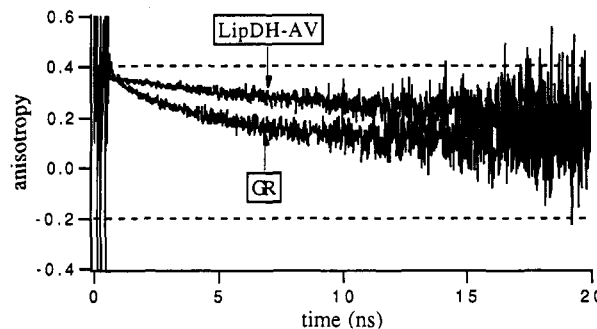

FIGURE 7: Experimental fluorescence anisotropy decays of LipDH-AV and GR in 50 mM potassium phosphate buffer at pH 7.0 and 293 K: excitation at 457.9 nm, emission at 550 nm. The broken lines indicate the theoretically possible values of the fluorescence anisotropy.

between conformational substates could not be determined but should be at least 1 order of magnitude larger than the enthalpy differences between states (slow exchange). The temperature invariance of the barycenter of the shortest lifetime component favors an interpretation based on an excited-state reaction, such as electron transfer from Tyr197 to the flavin in the first excited singlet (Visser et al., 1987; Kalman et al., 1991), over a dynamic quenching process caused by collision with the redox-active disulfide bridge (de Kok & Visser, 1987). This is also supported by the lifetime spectrum of the protein in 80% glycerol at 243 K (Figure 4B). If the origin of a short-lifetime component is due to dynamic quenching, one would expect that the barycenter would shift toward longer lifetimes at decreasing temperature and/or increase of viscosity since in these experimental conditions the frequency of protein fluctuations decreases. Such an effect is not observed.

Fluorescence Anisotropy Analysis. The fluorescence anisotropy decays of LipDH-AV and GR in aqueous solution at 293 K are shown in Figure 7. The rapid fluorescence anisotropy decline for GR, in contrast to LipDH-AV, is in agreement with previous results (de Kok & Visser, 1987). In the one-dimensional correlation time image of the fluorescence anisotropy decay of FAD bound to LipDH-AV, one can distinguish three regions of interest (Figure 8). At the flank of the spectrum with the highest ϕ values, an unresolved peak is apparent which indicates that the anisotropy levels to a constant value in the measured time window. From the size of the protein (100 kDa), one can calculate that the expected rotational correlation time from a modified Stokes–Einstein relation (Visser & Lee, 1980) is 38 ns at 20 °C. At all measured temperatures, this correlation time exceeds the fluorescence lifetimes by more than a factor of 10. In this case the intensity of the carrier signal (fluorescence decay)
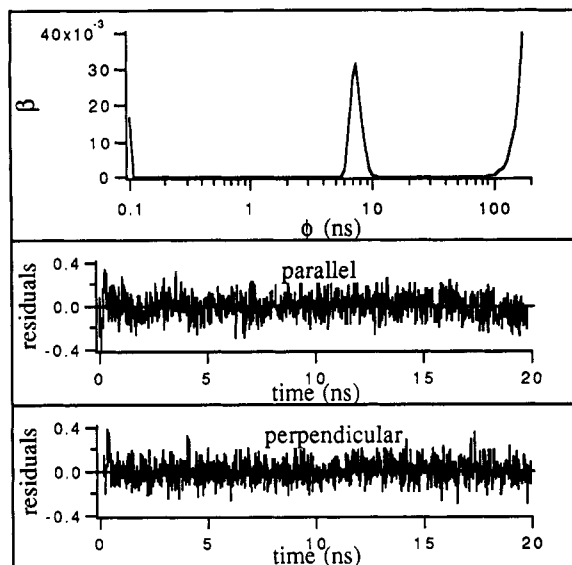
FIGURE 8: Correlation time spectrum of LipDH-AV in 50 mM potassium phosphate buffer at pH 7.0 and 283 K with the residuals of the fit to the parallel and perpendicular polarized fluorescence intensities.
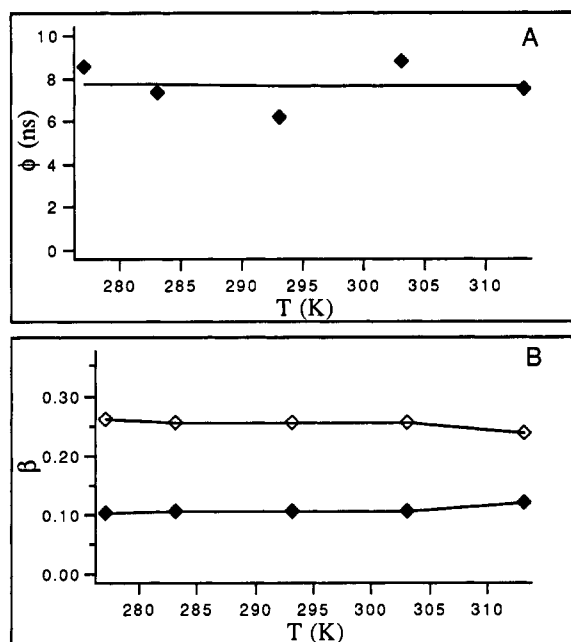

FIGURE 9: Temperature dependence of barycenters (A) and integrated amplitudes (B) as obtained from the correlation time spectra of LipDH-AV in 50 mM potassium phosphate buffer at pH 7.0: ◆, integrated amplitude and barycenter of process associated with energy transfer; ◇, integrated amplitude of limiting anisotropy.
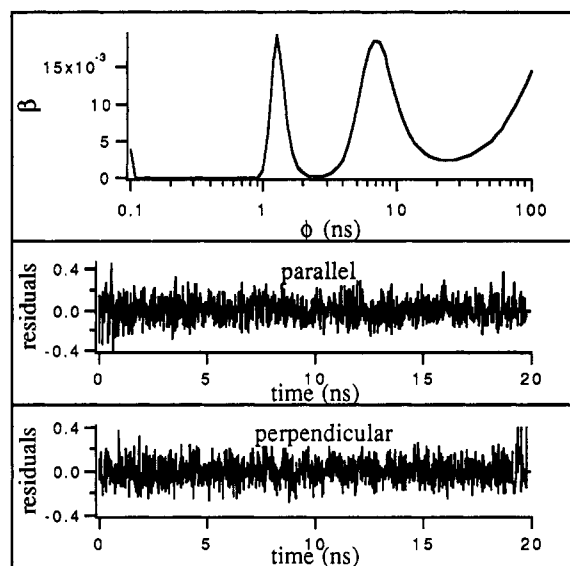

FIGURE 10: Correlation time spectrum of GR in 50 mM potassium phosphate buffer at pH 7.0 and 283 K with the residuals of the fit to the parallel and perpendicular polarized fluorescence intensities.
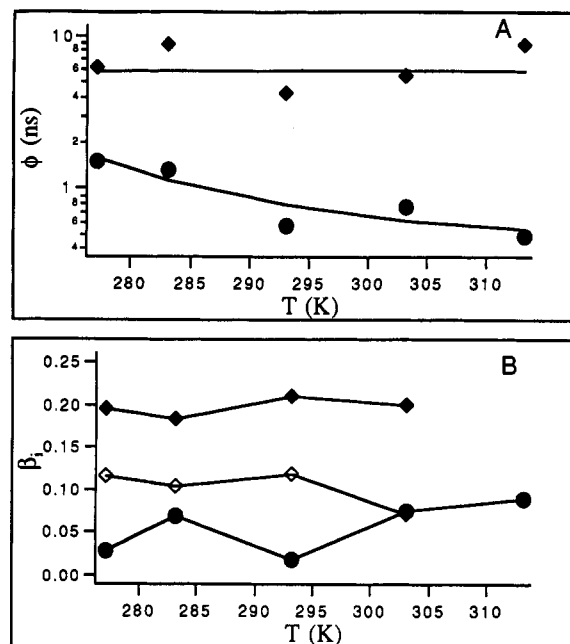

FIGURE 11: Temperature dependence of barycenters (A) and integrated amplitudes (B) as obtained from the correlation time spectra of GR in 50 mM potassium phosphate buffer at pH 7.0: ◆, integrated amplitude and barycenter of process associated with energy transfer; ●, integrated amplitude and barycenter of process associated with restricted motion; ◇, limiting anisotropy.

is too low on the time scale where protein rotation takes place. In the region between 6 and 9 ns, a peak could be resolved with a temperature-invariant barycenter and area (Figure 9A,B). The temperature invariance of this depolarizing process strongly suggests that it is not due to restricted reorientation of the flavins but to another depolarizing mechanism. The only other process which can then contribute to the depolarization of the fluorescence is intersubunit energy transfer between the flavins. As the overlap integral (J) was found to be temperature invariant between 277 and 313 K [J = (3.514 ± 0.088) × 10^{-15} M^{-1} cm^3], we also expect that the rate of this process will be invariant with temperature. At the extremely short correlation time flank of the spectrum, an unresolved peak is observed at all temperatures. The area under this peak has a value smaller than 0.02 at the measured

temperature interval and corresponds to an ultrafast depolarizing process not resolvable by our experimental system. We assign this process to rapid reorientational fluctuations with small amplitude (<5°) of the isoalloxazines within the protein matrix.

In the correlation time spectrum of GR, an additional peak is revealed at approximately 1.5 ns at 283 K that is not present in the spectrum of LipDH-AV (Figure 10). The barycenter of this peak shifts toward shorter correlation times upon increase of temperature (Figure 11A). This temperature dependence is an indication that the depolarizing process associated with this peak corresponds to restricted reorientational motion of the flavins. Similar to the spectrum of LipDH-AV, a temperature-invariant peak is present with a barycenter around 6 ns that again is associated with energy

Table I: Temperature-Invariant Parameters of Fluorescence Anisotropy Decays of LipDH-AV and GR

β_1	β_2	β_3	ϕ_T (ns)	global χ^2
	LipDH-AV			
	0.13[a]	0.23[a]	8.6[a]	1.10
	(0.11–0.17)	(0.18–0.25)	(6.2–14.8)	
	0.11[b]	0.25[b]	7.7[b]	
	(0.01)	(0.01)	(1.1)	
	GR			
0.10[a]	0.19[a]	0.08[a]	9.4[a]	1.25
(0.078–0.14)	(0.14–0.21)	(0.07–0.11)	(8.0–14.0)	
0.06[b]	0.20[b]	0.10[b]	6.5[b]	
(0.03)	(0.01)	(0.02)	(2.0)	

[a] Values as obtained from the global analysis of the parallel and perpendicular polarized fluorescence decays between 277 and 313 K. The numbers in parentheses are the errors at the 67% confidence level as determined from a rigorous error analysis. [b] Average values as obtained from the MEM analysis of the individual decay curves. The average was taken from the inverse Laplace transforms of the decays at five temperatures (277–313 K). The numbers in parentheses are the standard deviations.

transfer between the flavins. At 313 K, protein tumbling and energy transfer cannot be distinguished. The peak associated with energy transfer is then recovered as a shoulder in the spectrum. In this particular case, the relative amplitudes of both processes (energy transfer and protein tumbling) cannot be recovered. At the extreme short correlation time edge of the spectrum an ultrarapid depolarization is recovered at all temperatures (Figure 10). This process is not resolvable by our measuring system and probably corresponds to small-amplitude rapid reorientational fluctuations of the flavins, as in LipDH-AV. The areas of the different peaks remained constant within the measured temperature interval (Figure 11B), which shows that the angular parameters associated with different depolarizing processes (vide infra) are invariant.

The temperature invariance of the parameters describing the anisotropy decays of LipDH-AV and GR can be exploited by a global analysis. The temperature-invariant parameters can then be linked in the simultaneous analysis of the parallel and perpendicular polarized fluorescence decays at different temperatures. Since the inverse Laplace transform of the anisotropy decay of LipDH consisted of two peaks (energy transfer and protein tumbling), the anisotropy decays were modeled by a double-exponential function ($N = 2$):

$$r(t) = \sum_{i=1}^{N} \beta_i \exp(-t/\phi_i) \tag{9}$$

The preexponential amplitudes β_i were assumed to be invariant over the experimental temperature range and subsequently linked in the simultaneous analysis of the temperature-dependent polarized fluorescence decays. The temperature-invariant correlation time associated with energy transfer was also linked over all experiments. In the global analysis of the polarized fluorescence of GR, the anisotropy decays were modeled by a triple-exponential function (eq 9, $N = 3$). The β_i were assumed invariant to temperature and linked over all experiments. The correlation time associated with energy transfer was again interlinked but not the correlation time associated with restricted motion. The values of the temperature-invariant parameters obtained after global and MEM analyses of the polarized fluorescence decays are collected in Table I together with the error estimates at the 67% confidence level. The global fit of the polarized fluorescence decays of the proteins at five temperatures (277–313 K) was satisfactory, as judged by the random distribution of residuals around zero except for a small nonrandom deviation at short times (Figure
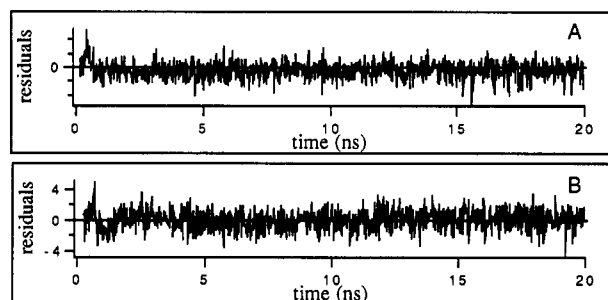

FIGURE 12: Residuals of global fit of anisotropy decays of LipDH-AV (A) and GR (B). Mark the deviations at short times due to an unresolvable ultrafast depolarization process. Only the residuals of the fit of the anisotropy decays at 293 K are shown.

12). This ultrarapid depolarization observed both in GR and LipDH-AV which was resolved by MEM could not be fitted by the global analysis program even by addition of an extra exponential term in the decay model (eq 9, $N = 4$). Since this process has a small amplitude and is outside the time domain (few picoseconds) of our interest, it was further neglected in the analysis of the anisotropy decays. It should be noted, however, that the global χ^2 is somewhat higher than unity by exclusion of this ultrarapid process in the analysis.

With eq A5 of the Appendix we can relate the empirical parameters (ϕ_i, β_i) of the anisotropy decay model of GR to geometrical parameters of the protein. The integral of amplitudes associated with restricted reorientational motion is β_1, the integral of amplitudes associated with energy transfer is β_2, and the integral of peak amplitudes associated with protein tumbling is β_3 (limiting anisotropy). By expanding the Legendre polynomials in eq A5 and by algebraic manipulation of the preexponential amplitudes we obtain

$$\beta_1 + \beta_2 + \beta_3 = \frac{3}{5}\cos^2\delta - \frac{1}{5} \tag{10}$$

$$\frac{\beta_2 + \beta_3}{\beta_1 + \beta_2 + \beta_3} = 1 - \frac{\beta_1}{\beta_1 + \beta_2 + \beta_3} = S^2 \tag{11}$$

$$\frac{\beta_3 - \beta_2}{\beta_2 + \beta_3} = \frac{3}{2}\cos^2\theta - \frac{1}{2} \tag{12}$$

where δ is the intramolecular angle between absorption and emission transition moments and θ is the intermolecular angle between the symmetry axes of the potential wells. The second rank order parameter S can be related to a maximal cone semiangle of reorientation (ψ) following the a priori solution of Kinosita et al. (1977):

$$S = \sqrt{\frac{1}{2}\cos\psi\,(\cos\psi + 1)} \tag{13}$$

From the correlation time of restricted motion (ϕ_M) one obtains the diffusion coefficient ($D_\perp$) at temperature T:

$$D_\perp = (1 - S^2)/6\phi_M \tag{14}$$

and from the correlation time associated with energy transfer (ϕ_T) the rate of transfer (k_T)

$$k_T = 1/2\phi_T \tag{15}$$

The preexponential amplitudes of the anisotropy decay model of LipDH-AV can only be related to geometrical parameters describing the relative isoalloxazine orientation in both subunits. By expansion of the Legendre polynomials in eq A6

Table II: Geometrical Parameters and Inter-Flavin Energy-Transfer Rate Constant of LipDH-AV and GR

S	ψ (deg)	θ (deg)	δ (deg)	k_T (MHz)	R (mm)
		LipDH-AV			
		134^a	15^a	58^a	3.7^a
		(125–139)	(15–16)	(36–81)	(3.5–4.0)
		139^b	15^b	65^b	3.6^b
		(2)	(1)	(9)	(0.1)
		GR			
0.85^a	36^a	104^a	13^a	53^a	3.7^a
(0.79–0.91)	(28–44)	(101–120)	(10–14)	(36–63)	(3.6–4.0)
0.92^b	27^b	111^b	16^b	77^b	3.5^b
(0.05)	(9)	(8)	(2)	(23)	(0.2)

[a] Values as calculated from the parameters obtained after a global analysis of the parallel and perpendicular polarized fluorescence decays between 277 and 313 K. The numbers in parentheses are the errors at the 67% confidence level as determined from a rigorous error analysis. [b] Average values as calculated from the average parameters of a MEM analysis of the individual decay curves. The average was taken from the inverse Laplace transforms of the decays at five temperatures (277–313 K). The numbers in parentheses are the standard deviations.

of the Appendix and after addition and subtraction of the preexponential amplitudes, we obtain

$$\beta_2 + \beta_3 = \frac{3}{5}\cos^2\delta - \frac{1}{5} \tag{16}$$

$$\beta_3 - \beta_2 = \frac{3}{5}\langle\cos^2\theta\rangle - \frac{1}{5} \tag{17}$$

θ is now the intermolecular angle between absorption and emission transition moments. In eq 17 the brackets denote an average over two angles which are not necessarily the same: θ_1, the angle between the emission transition moment in isoalloxazine 1 and the absorption transition moment in isoalloxazine 2 and θ_2, the angle between the emission transition moment in isoalloxazine 2 and the absorption transition moment in isoalloxazine 1. As we cannot distinguish the direction of transfer in the correlation time spectrum of LipDH-AV (unimodal peak), θ_1 and θ_2 are taken as approximately equal. The geometrical parameters and the rate of transfer as calculated from the anisotropy decay parameters obtained after global and MEM analyses of the anistropy decays are collected in Table II. From eq 17, one obtains two solutions for the intermolecular angle (θ) between transition moments. In Table II are collected the solutions which are in agreement with the C_2 symmetry of LipDH-AV and GR. In GR we found evidence for reorientational motion of the flavins. When this motion is modeled as diffusive motion within a box with infinitely high potential walls, we found a cone semiangle between 28° and 44°. The diffusion constant ($D_\perp$) as calculated with eq 14 increases with temperature as expected for a temperature-dependent process such as reorientational motion (Figure 13). Since reorientational motion of the flavins takes place in GR, the intermolecular angle (θ) is the angle between the symmetry axes of the potential wells. It is reasonable to assume that in the crystal structure the flavins are immobilized in an energy state corresponding to the minimum of a potential well. In that case, the flavins are oriented with their pseudosymmetry axes parallel to the symmetry axes of the potentials. The angle θ as obtained from crystallographic coordinates (Karplus & Schulz, 1987) is then 102°, which is also in agreement with the angle as obtained from fluorescence depolarization (Table II).

The intermolecular angle between absorption and emission transition moments in the immobilized isoalloxazines (θ) of
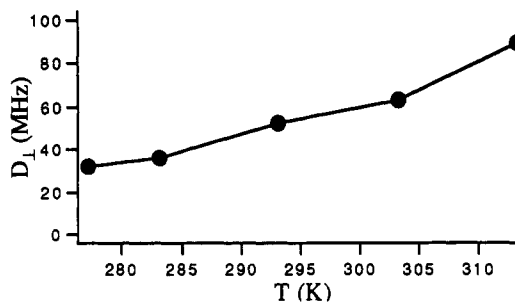

FIGURE 13: Perpendicular diffusion constant of reorientational motion of flavins bound to GR as function of temperature.
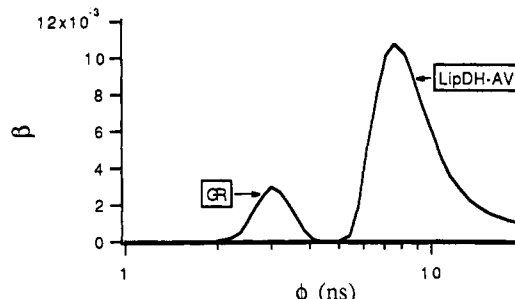

FIGURE 14: Correlation time spectrum of LipDH-AV and GR in 80% glycerol, 50 mM potassium phosphate buffer at pH 7.0 at 243 K. For clarity only the region between 1 and 20 ns is shown.

LipDH-AV is in accordance with the value as calculated from crystallographic coordinates (138°) (Mattevi et al., 1991). The intermolecular distances between the isoalloxazines as obtained from the Förster equation with the orientation factor κ^2 as calculated from crystallographic data (Table II) are in excellent agreement with those directly calculated from the crystal structures (3.9 nm for both GR and LipDH-AV). The correspondence between crystallographic geometry and that derived from optical spectroscopy shows that our interpretation of the fluorescence anisotropy is correct in both proteins.

A single peak with a limiting anisotropy was obtained for the proteins at 243 K in 80% glycerol (Figure 14). Restricted reorientational motion is then completely inhibited in the proteins, and the sole mechanism responsible for fluorescence depolarization is energy transfer. It should be noted that the integrated amplitude of the energy-transfer peak for GR in 80% glycerol is much lower than in aqueous solution (see Discussion). The angles θ and δ and the interflavin distance as calculated from the parameters obtained from a global analysis of the anisotropy decays of LipDH-AV in 80% glycerol at different temperatures ($\theta = 139°$, $\delta = 17°$, R = 3.8–4.2 nm) correspond well with those obtained in aqueous solution (Table II), which confirms that energy transfer is indeed the major cause for the depolarization of the fluorescence in LipDH-AV. Details of this analysis are presented elsewhere (Bastiaens et al., 1992b). Restricted motion of the flavins in GR is completely abolished in 80% (v/v) glycerol at 243 K. The sole mechanism of depolarization is then energy transfer between the cofactors. The model of energy transfer has to be modified as compared to the one in aqueous solution. The recovered angle θ is now the intermolecular angle between transition moments instead of the intermolecular angle between symmetry axes of the potential wells. The angle θ, as obtained from the fluorescence depolarization experiment ($\theta = 158°$), is larger than the angle found in LipDH-AV. The subunits possibly have different mutual orientations in both proteins. The angle θ as obtained from crystallographic data ($\theta = 148°$ for GR instead of 138° for LipDH-AV) corroborates this finding. The fluorometric θ is comparable to the intermo-

lecular angle between absorption transition moments (163°). The question then arises whether the intramolecular angle δ is not overestimated because of rapid reorientational fluctuations of the flavins on a time scale beyond the resolution of the experimental system.

DISCUSSION

Comparison of the thermal behavior of the fluorescence kinetics of GR and LipDH-AV shows that the conformational dynamics differ to a large extent. The temperature invariance of the lifetimes in GR indicates that the activation energies between conformational substates are larger than in LipDH-AV. Almost 90% of GR is in a state with an extremely short fluorescence lifetime (30 ps) of the flavin. The rapid depopulation of the flavin excited state arises from exciplex formation with Tyr197, a residue absent in LipDH-AV. The other (minor) components probably originate from conformational substates where the relative positioning of Tyr197 and isoalloxazine is unfavorable for efficient electron transfer. It has been proposed that Tyr197 functions as a lid to protect the two-electron-reduced enzyme against oxidation (Pai & Schulz, 1983). It is possible that equilibrium fluctuations between conformations with different orientations of the "lid" correspond to the observed five lifetime classes. The increase in relative populations associated with the longer lifetime components, observed in 80% glycerol GR solution, can be accounted for by a decreased stacking interaction between the isoalloxazine and tyrosine rings. The "open" conformation of the enzyme is thus more stabilized in 80% glycerol. Since the activation barriers between conformational substates are large in GR (on the order of 100 kJ/mol or larger), the transitions between states, with different orientations of Tyr197, correspond to gross structural changes in the protein. Confirmation that large structural changes are involved in closing the active site came from site-directed mutagenesis on GR from *E. coli* (Berry et al., 1989). In these studies the tyrosine had been replaced by glycine with maintenance of the protection against oxidation of the two-electron-reduced enzyme. It was concluded that the flavin is buried within the protein in the "closed" form.

We can propose a role in catalysis of equilibrium fluctuations between conformational states in GR and LipDH-AV. With time-resolved fluorescence spectroscopy, 90% of GR was found to exist in a conformation where the flavin has a tight interaction with Tyr197 (closed conformation). In this conformation, the prosthetic group is not accessible for NADPH and cannot form a productive binary complex. In the remaining fraction (<10%), the tyrosine is displaced and the enzyme is in a proper state to bind NADPH (open conformation). The protein in this conformation (without coenzyme) has the same spatial structure as the binary complex. When NADPH binds to this "open conformation", the equilibrium is shifted to the enzyme–substrate complex. Equilibrium between conformational substates is then reestablished to repeat the binding cycle. In this model, binding of the coenzyme is only possible when the appropriate open enzyme conformation is preexisting. Such a mechanism is in contrast to a model where a conformational change is induced by binding of the coenzyme to the closed form of the enzyme. Since large activation barriers prevail between conformational substates, the rate-limiting step of cofactor binding could well be the conformational transition from closed to open enzyme forms.

From fluorescence quenching and solvent relaxation experiments, we obtained evidence that the flavin is not accessible to solvent in the majority of LipDH-AV molecules (Bastiaens et al., 1992a). In contrast, in a deletion mutant lacking 14 amino acids at the C-terminus, the flavins are partly exposed to the solvent. It can be envisioned that this terminal peptide has a lid function, preventing electrons from entering the flavin site in most of the enzymes. A minor fraction of LipDH-AV molecules possibly exists in an open conformation ready to bind substrate [Lip(SH)$_2$]. The shortest component (150 ps) in the lifetime spectrum is a possible manifestation for this more open protein conformation since it has the lowest contribution. Additional time-resolved fluorescence quenching experiments should be carried out to prove this point. We can then tentatively assign a role in catalysis to equilibrium fluctuations between conformational substates in LipDH-AV similar to that in GR. In LipDH-AV, however, the interconversion between substates at 293 K is much more rapid than in GR, ruling out the possibility this transition is the rate-limiting step in substrate binding.

In previous studies, the anisotropy decay of LipDH was fitted to double-exponential decay functions. The two correlation times were interpreted as arising from restricted hinge motion of the subunits and protein tumbling (Bosma et al., 1982; de Kok & Visser, 1984, 1987). From the analysis of the anisotropy decay with the one-dimensional version of MEM, we obtained a unimodal distribution of correlation times with a limiting anisotropy. The information on the rotational correlation time of protein tumbling is thus highly uncertain and cannot be extracted from the data (Figures 8 and 10). The temperature invariance of the barycenter and of the integrated amplitude of the unimodal peak in the correlation time spectrum firmly establishes that the underlying physical mechanism of depolarization is intersubunit energy transfer between the flavins. Additional evidence for this mechanism is obtained from the correlation time spectrum of LipDH-AV in 80% glycerol at 243 K. The unimodal peak is also present with similar barycenter and amplitude. The geometrical parameters, as derived from the global analysis of the fluorescence anisotropy decays at five temperatures according to an energy-transfer model, are in agreement with crystallographic data. The flavins are thus rigidly bound and only ultrarapid reorientational fluctuations of small amplitude ($\psi < 5°$) can be detected. The rapid exchange between conformational substates at temperatures above 283 K is then not associated with an angular displacement of the flavins. The equilibrium fluctuations of the conformational substate correspond to a rearrangement of the flavins' environment without changing their relative orientation.

A bimodal correlation time distribution and a limiting anisotropy is found for GR instead of the reported monoexponential decay function (de Kok & Visser, 1987). By the temperature invariance of the peak located at around 6 ns we could demonstrate that a considerable contribution to the depolarization originates from energy transfer between the flavins. In addition to energy transfer, restricted reorientational motion of the flavins is observed in contrast to the situation in LipDH-AV. Despite the small angular displacement of the flavins (22–44°), almost complete depolarization of the fluorescence is observed for this protein. Energy transfer is then the major contributor to the depolarization. The large peak amplitude of this process has two origins: (i) the second rank order parameter contributes to the amplitude of the peak (eq A5), and (ii) the angle between symmetry axes of the flavin potential wells is smaller than the angle between the transition moments in the immobilized state (104° instead of 158°). The latter point is exemplified by the fluorescence

depolarization of GR in 80% glycerol at 243 K. Restricted motion is then abolished, and the sole mechanism of depolarization is energy transfer. The integrated amplitude of the peak associated with energy transfer is in that case about a factor of 6–7 smaller than in aqueous solution.

The flexibility of the flavins in GR is in sharp contrast with the highly immobilized isoalloxazines as found in the crystal structure (Karplus & Schulz, 1987). The majority of the ensemble of enzymes (90%) have a conformation where the lifetime of the flavins is about 30 ps. The excited state of the flavin in this (large) fraction of molecules is depopulated before any depolarization due to restricted motion or energy transfer can take place. Because of this short lifetime, one cannot decide on the dynamic properties of this population. This conformational substate could thus be highly rigid, as observed in the crystal structure. The carrier signal for depolarization comes from the longer lived components, which correspond to protein populations with an unfavorable conformation for the formation of the flavin–tyrosine exciplex. As can be envisioned, the flavin is flexible in these conformations because of the alleviation of the spatial constraints of the proximal tyrosine.

Owing to the high dynamic range and nanosecond observation window in time-resolved fluorescence, in conjunction with the unequivocal lifetime distribution analysis, it is possible to monitor minor fractions of protein conformational substates. Temperature-dependent fluorescence relaxation spectroscopy provides us therefore with a powerful tool to investigate the role of conformational dynamics in flavoprotein catalysis. In addition, the factors contributing to the depolarization of the fluorescence can be quantitatively separated. In this way, reliable geometric information in multichromophoric proteins in solution can be obtained.

ACKNOWLEDGMENT

APPENDIX

Quantitative Interpretation of Fluorescence Anisotropy Decay. The proteins have distinct structural and dynamic properties. In LipDH-AV energy transfer is the main cause for fluorescence depolarization whereas additional restricted reorientational motion takes place in GR. In order to find useful expressions which relate the inverse Laplace transform of the anisotropy decays to physical parameters, one has to adopt reasonable assumptions about the system under investigation. Our first assumption is that the decay of the excited state is independent of the orientation of the molecules in the protein matrix. In this case, the electronic and orientational states of a molecule are uncoupled (nonassociative modeling). The master equation relating the anisotropy decay [$r(t)$] to the orientational correlation function is then (Zannoni, 1981; Szabo, 1984)]

$$r(t) = \ll P_2[\vec{u}_a \cdot \vec{u}_e(t)] \gg \qquad (A1)$$

where $\vec{u}_a$ and $\vec{u}_e$ are unit vectors pointing along the absorption and emission transition moments of the flavin molecule, respectively. P_2 denotes a second-order Legendre polynomial, and the brackets ($\ll \gg$) indicate a molecular ensemble average. In a system where restricted reorientational motion takes place together with energy transfer (e.g., in GR), the contributions of the individual processes to the depolarization can be factorized into a Soleillet product when restricted

motion takes place on a faster time scale than energy transfer (Soleillet, 1929):

$$r(t) = \frac{2}{5}P_2(\cos \delta)C_M C_T \qquad (A2)$$

where C_M and C_T are the correlation functions of (restricted) motion and (energy) transfer, repectively, and δ is the angle between the absorption and emission transition moments within a flavin molecule. In order to obtain an analytical expression for the reorientational correlation function, one has to consider (i) the potential well in which the flavin reorients and (ii) the type of dynamics (strong collision or diffusion model). In order to quantify our data, we have chosen a simple model based on a uniaxial potential with diffusive dynamics for flavin reorientation. The single-exponential approximation of van der Meer et al. (1984) describes such a system:

$$C_M = [1 - S^2] \exp[-6D_\perp t/(1 - S^2)] + S^2 \qquad (A3)$$

where S is the second rank order parameter and $D_\perp$ (ns^{-1}) the diffusion coefficient perpendicular to the symmetry axis of the potential well. It is to be noted that this expression can be replaced by another type of model describing reorientational dynamics [e.g., jump (Zannoni, 1981) or more refined diffusion models (Szabo, 1984; van der Meer et al., 1984)]. In eq A3, the position of the emission transition moment is assumed to be approximately parallel to the flavin (pseudo) symmetry axis. The analytical expression for the transfer correlation function has been derived and is exact (Tanaka & Mataga, 1979):

$$C_T = \frac{1}{2}[[1 - P_2(\vec{D}_1 \cdot \vec{D}_2)] \exp[-2k_T t] + P_2(\vec{D}_1 \cdot \vec{D}_2) + 1] \qquad (A4)$$

where k_T is the rate of intermolecular Förster energy transfer. Since the transition moments are completely randomized within the potential well, this expression does not contain the angular parameters describing the mutual orientation of the absorption and emission transition moments. The angular parameter which is contained in the preexponential amplitudes in eq A4 is the angle between the symmetry axes ($\vec{D}_i$) of the potentials. After substitution of eqs A3 and A4 into eq A2, an expression for the time-dependent anisotropy for a system where restricted motion and energy transfer contribute to the depolarization of the fluorescence is obtained:

$$r(t) = \frac{2}{5}P_2(\cos \delta)\left\{[1 - S^2] \exp\left[\frac{-6D_\perp t}{1 - S^2}\right] + \frac{1}{2}S^2 \times \right.$$
$$\left. [1 - P_2(\vec{D}_1 \cdot \vec{D}_2)] \exp[-2k_T t] + \frac{1}{2}S^2[1 + P_2(\vec{D}_1 \cdot \vec{D}_2)]\right\} \qquad (A5)$$

For a system of two chromophores with fixed unique orientation interacting by the Förster mechanism (as in LipDH-AV), the time-dependent anisotropy is described by (Tanaka, & Mataga, 1979)

$$r(t) = \frac{1}{10}\{2P_2(\vec{\mu}_a^1 \cdot \vec{\mu}_e^1) + P_2(\vec{\mu}_a^1 \cdot \vec{\mu}_e^2) + P_2(\vec{\mu}_a^2 \cdot \vec{\mu}_e^1) +$$
$$[2P_2(\vec{\mu}_a^1 \cdot \vec{\mu}_e^1) - P_2(\vec{\mu}_a^1 \cdot \vec{\mu}_e^2) - P_2(\vec{\mu}_a^2 \cdot \vec{\mu}_e^1)] \exp[-2k_T t]\} \qquad (A6)$$

The preexponential amplitudes now contain information on the inter- and intramolecular angles between absorption and emission transition moments in the dimeric homotransfer system.

REFERENCES

Alcala, R. J., Gratton, E., & Prendergast, F. G. (1987) *Biophys. J. 51*, 597–604.

Ameloot, M., Beechem, J. M., & Brand, L. (1986) *Chem. Phys. Lett. 129*, 211–219.

Austin, R. H., Beeson, K. W., Eisenstein, L., Frauenfelder, H., & Gunsalus, I. C. (1975) *Biochemistry 14*, 5355–5373.

Bastiaens, P. I. H., Bonants, P. J. M., van Hoek, A., Müller, F., & Visser, A. J. W. G. (1988) *Proc. SPIE 909*, 257–262.

Bastiaens, P. I. H., Bonants, P. J. M., Müller, F., & Visser, A. J. W. G. (1989) *Biochemistry 28*, 8416–8425.

Bastiaens, P. I. H., Mayhew, S. G., O'Nualláin, E. M., van Hoek, A., & Visser, A. J. W. G. (1991) *J. Fluoresc. 1*, 95–103.

Bastiaens, P. I. H., van Hoek, A., van Berkel, W. J. H., de Kok, A., & Visser, A. J. W. G. (1992a) *Biochemistry* (following paper in this issue).

Bastiaens, P. I. H., van Hoek, A., Benen, J. A. E., Brochon, J. C., & Visser, A. J. W. G. (1992b) *Biophys. J.* (in press).

Beechem, J. M., & Brand, L. (1985) *Annu. Rev. Biochem. 54*, 43–71.

Beechem, J. M., & Gratton, E. (1988) *Proc. SPIE 909*, 70–81.

Beechem, J. M., Gratton, E., Ameloot, M., Knutson, J. R., & Brand, L. (1991) The global analysis of fluorescence intensity and anisotropy decay data, in *Topics in Fluorescence Spectroscopy* (Lakowicz, J. R., Ed.) Vol. 2, pp 241–305, Plenum Press, New York.

Berry, A., Scrutton, N. S., & Perham, R. N. (1989) *Biochemistry 28*, 1264–1269.

Boens, N., Janssens, L. D., & de Schryver, F. C. (1989) *Biophys. Chem. 33*, 77–90.

Bosma, H. J., de Graaf-Hess, A. C., de Kok, A., Veeger, C., Visser, A. J. W. G., & Voordouw, G. (1982) *Ann. N.Y. Acad. Sci. 378*, 265–286.

de Kok, A., & Visser, A. J. W. G. (1984) in *Flavins and Flavoproteins* (Bray, R. C., Engel, P. C., & Mayhew, S. G., Eds.) pp 149–152, Walter de Gruyter, Berlin.

de Kok, A., & Visser, A. J. W. G. (1987) *FEBS Lett. 218*, 135–138.

Frauenfelder, H., & Gratton, E. (1986) *Methods Enzymol. 127*, 207–216.

Frauenfelder, H., Parak, F., & Young, R. D. (1988) *Annu. Rev. Biophys. Biophys. Chem. 17*, 451–479.

Gavish, B., & Werber, M. M. (1979) *Biochemistry 18*, 1269–1275.

Kalman, B., Sandström, A., Johansson, L. B.-A. & Lindskog, S. (1991) *Biochemistry 30*, 111–117.

Kalse, J. F., & Veeger, C. (1968) *Biochim. Biophys. Acta 159*, 244–256.

Karplus, P. A., & Schulz, G. E. (1987) *J. Mol. Biol. 195*, 701–729.

Kinosita, K., Kawato, S., & Ikegami, A. (1977) *Biophys. J. 20*, 289–305.

Krohne-Ehrich, G., Schirmer, R. H., & Untucht-Grau, R. (1971) *Eur. J. Biochem. 80*, 65–71.

Livesey, A. K., & Brochon, J. C. (1987) *Biophys. J. 52*, 693–706.

Mattevi, A., Schierbeek, J. A., & Hol, W. G. J. (1991) *J. Mol. Biol. 220*, 975–994.

Mérola, F., Rigler, R., Holmgren, A., & Brochon, J. C. (1989) *Biochemistry 28*, 3383–3398.

O'Connor, D. V., & Phillips, D. (1984) *Time-Correlated Single Photon Counting*, Academic Press, London.

Pai, E. F., & Schulz, E. (1983) *J. Biol. Chem. 258*, 1752–1757.

Reed, L. J. (1974) *Acc. Chem. Res. 7*, 40–46.

Schierbeek, A. J., Swarte, M. B. A., Dijkstra, B. W., Vriend, G., Read, R. J., Hol, W. G. J., Drenth, J., & Betzel, C. (1989) *J. Mol. Biol. 206*, 365–379.

Schulz, G. E., Zappa, H., Worthington, D. J., & Rosemeyer, M. A. (1975) *FEBS Lett. 54*, 86–88.

Schulze, E., Benen, J. A. E., Westphal, A. H., & de Kok, A. (1991) *Eur. J. Biochem. 200*, 29–34.

Soleillet, P. (1929) *Ann. Phys. X 12*, 23–97.

Szabo, A. (1984) *J. Chem. Phys. 81*, 150–167.

Tanaka, F., & Mataga, N. (1979) *Photochem. Photobiol. 29*, 1091–1097.

van Berkel, W. J. H., Benen, J. A. E., & Snoek, M. C. (1991) *Eur. J. Biochem. 197*, 769–779.

van der Meer, W., Pottel, H., Herreman, W., Ameloot, M., Hendrickx, H., & Schröder, H. (1984) *Biophys. J. 46*, 515–523.

van Hoek, A., Vos, K., & Visser, A. J. W. G. (1987) *IEEE J. Quantum Electron. QE-23*, 1812–1820.

Visser, A. J. W. G., & Lee, J. (1980) *Biochemistry 19*, 4366–4372.

Visser, A. J. W. G., van Hoek, A., Kulinski, T., & LeGall, J. (1987) *FEBS Lett. 224*, 406–410.

Westphal, A. H., & de Kok, A. (1988) *Eur. J. Biochem. 172*, 299–305.

Williams, C. H. J. (1976) *Enzymes (3rd Ed.) 13*, 89–173.

Worthington, D. J., & Rosemeyer, M. A. (1974) *Eur. J. Biochem. 48*, 167–177.

Zannoni, C. (1981) *Mol. Phys. 42*, 1303–1320.